1-25-2022

Molecular Dynamic Simulation of Diffusion in the Melt Pool in Laser Additive Alloying Process of Co-Ni-Cr-Mn-Fe High Entropy Alloy

Mathew Farias

Han Hu

Shanshan Zhang

Jianzhi Li

Ben Xu

Proceedings of the ASME 2021
International Mechanical Engineering Congress and Exposition
IMECE2021
November 1-5, 2021, Virtual, Online

IMECE2021-72075

MOLECULAR DYNAMIC SIMULATION OF DIFFUSION IN THE MELT POOL IN LASER ADDITIVE ALLOYING PROCESS OF CO-NI-CR-MN-FE HIGH ENTROPY ALLOY

Mathew Farias
Depart. of Manufacturing and Industrial Engineering, The University of Texas Rio Grande Valley, Edinburg, TX 78539

Han Hu
Depart. of Mechanical Engineering, University of Arkansas, Fayetteville, AR 72701

Shanshan Zhang
Depart. of Manufacturing and Industrial Engineering, The University of Texas Rio Grande Valley, Edinburg, TX 78539

Jianzhi Li
Depart. of Manufacturing and Industrial Engineering, The University of Texas Rio Grande Valley, Edinburg, TX 78539

Ben Xu*
Depart. of Mechanical Engineering, Mississippi State University, Mississippi State, MS 39762
xu@me.msstate.edu

ABSTRACT

High entropy alloys (HEAs) can be manufactured in many conventional ways, but it becomes difficult of fabricating heterogeneous materials and structures. Selective Laser Melting (SLM) method generally melts pure elemental powders or prefabricated alloy powders without alloying process. *In-situ* alloying in SLM, which is also called Laser Additive Alloying (LAA), using pure elemental powders becomes a promising method for creating HEA with heterogeneous structures. However, the effect of the diffusion of elements in the molten pool on the formation of HEA remains unclear. In this paper, the well-discussed Cantor HEA was studied in an *in-situ* alloying situation, where pure elemental powders (Co, Cr, Mn, Ni, Fe) distributed on a powder bed were irradiated by laser and were subsequently allowed to cool back to room temperature. The diffusion of specific elements, with respect to their original clusters, was tracked via Mean Square Displacement (MSD) as well as the final composition of key locations. Our model was verified by showing a good agreement with the overall average diffusion rates of each element in the Cantor HEA qualitatively in other works from literature. Results initially showed that as the energy density increases, better diffusion was observed through a pixel overlay analysis about the mixing of different elements. The best-case scenario of diffusion from the pixel overlay map indicated a strong presence of 3 to 4 elements after the laser scanning. Given the conditions in the MD simulation, there was no apparent segregation of elements during the alloying process. In addition, we also conducted a simulation by implementing a 0.03 nm/ps laser scanning in a meander 2-track scan in order to completely melt the powder bed. After cooling and equilibration, Polyhedral Template Analysis was applied to analyze the crystal structure of the solidified powder bed in the presence of increasing components. When the powders of Cantor HEA were alloyed using LAA approach, all elements experienced a complex diffusion behavior, elements like Cr also experienced a relatively rapid diffusion compared to other elements. Despite this, Cr only diffused for a short period and diffused minimally during the *in-situ* alloying process. The analysis of element-specific behavior, such as diffusion, can provide a framework for the LAA production of HEA. This MD study provides a detailed analysis about the effect of diffusion on the formation of HEA system if *in-situ* alloying is adopted, the findings of this study can be used to guide the material design and the appropriate parameters for manufacturing process of new HEAs. This study can also be extended to analyze the effect of diffusion on the thermomechanical properties of HEAs.

Key Words: Molecular Dynamics (MD), High Entropy Alloy (HEA), Laser Additive Alloying (LAA), Selective Laser Melting (SLM), Additive Manufacturing (AM).

1. INTRODUCTION

High entropy alloys (HEAs) are composed of 5 or more principal components at near equal atomic composition [1]. The name HEA was first coined by Yeh *et al.* [2], the subset of alloys would be also simultaneously referred to as multi-component alloys by Cantor *et al.* [3]. HEA can exhibit exemplary material properties, such as high wear resistance [4], high-temperature strength [5], high hardness [6], and corrosion resistance depending [7] on what constituent element the system is made of

and its crystal structure [1, 8]. Many studies attribute these properties to the hypothesis of high lattice distortion exhibited in such alloys [9, 10]. The Cantor HEA, Co-Cr-Mn-Ni-Fe, is the most studied HEA, and it is largely considered ideal as it is known to create a single disordered solid solution with an FCC crystal structure [11].

Selective Laser Melting (SLM) is an additive manufacturing (AM) process that has drawn much attention. The SLM process involves powder distributed along a substrate which is subsequently selectively melted by a scanning laser. SLM can create complex near-net-shape products provided the material powders and a STereoLithography (STL) file. The mixing process in the SLM melt pool is a rapid melting and freezing process that is largely driven by Marangoni force, and other material properties, such as viscosity, density, and melting temperatures [12]. SLM method generally melts pure elemental powders or prefabricated alloy powders without alloying process. However, *in-situ* alloying of pure elemental powders during the SLM process allows for the freedom to create alloys with high degrees of customization and as such is a promising method for creating HEA, especially for fabricating the heterogeneous structures and changing material properties by adding additional elements in the original HEA system. However, much is unknown about the diffusion process occurring in the melt pool and its effects on the formation of HEA and other properties if in-situ alloy is adopted to fabricate the HEA. Moreover, the empirical methods that have been used to calculate diffusion coefficients in HEA have been proven to be a source of controversy [13-15].

Molecular Dynamics (MD) provides a unique numerical framework to measure the atomic transport in the powder bed, since studying the rapid melting and cooling SLM process experimentally could be an arduous task. However, atomistic studies performed on MD software have been able to mimic AM methods such as selective laser sintering (SLS) [16-18] and SLM [19]. MD can be used to predict the formation, segregation, and mobility in a crystal lattice at an atomic level [17, 20, 23]. Inspired by these works, MD simulation can be applied to explore the mobility of atoms in the Cantor HEA powder bed, the behavior occurring in both the rapidly melting and freezing melt pool, the effects of laser parameters on the formation of HEA, and the feasibility of its production in the SLM process can be studied. In this paper, the diffusion behavior of atoms in the powder bed was studied after interaction with a rapid scanning laser. Initial studies focused solely upon identifying trends in the diffusion of specific elements in the powder bed, and a single laser scan with varying energy densities was chosen. An attempt was made to determine the "hotspots" of diffusion with excellent powder mixing after melting. To fully melt the powders in the powder bed, a second laser track was adopted, and the effects of energy drift and the final crystal structure were compared with the results of single laser track. This study aims to provide an MD analysis about the effect of diffusion on the formation of HEA system if adopting *in-situ* alloying of pure elemental powders, the results obtained in this MD study can be used to guide the design of new HEA system using LAA approach, the findings of this study can be used to guide the material design and the appropriate parameters for manufacturing process of new HEAs. This study can also be extended to analyze the effect of diffusion on the thermomechanical properties of HEAs.

2. METHODOLOGY AND SIMULATION SETUP

All MD simulations were performed using the Large-scale Atomic/Molecular Massively Parallel Simulator (LAMMPS) open-source software [22, 23] and visualized using OVITO [26]. The study incorporated 121,524 atoms: 104,196 Fe atoms (including both substrate and powder atoms), 3860 Cr atoms, 4576 Ni atoms, 4468 Co atoms, and 4424 Mn atoms. The simulation domain can be found in Figure 1, where the domain was designed specifically to avoid any adjacent duplicate elemental powders, and the powders were also situated far from the x and y boundaries to isolate the simulation. To simplify the model, all powder diameters were chosen to be the same, due to varying lattice parameters, atoms per powder vary with each element. Simulations were performed using a modified embedded atom method (MEAM) developed as a generalization of the embedded atom method (EAM) where total energy is described as:

$$E = \sum_i \{F_i(\bar{\rho}_i) + \frac{1}{2}\sum_{i \neq j} \emptyset_{ij}(r_{ij}) \quad (1)$$

where r_{ij} is the distance between a given body and its neighbor, $\emptyset$ is pair potential function between atom pairs, and F is an embedding energy that is a function of ρ or electron density.

The MEAM potential was chosen from the NIST repository as a result of studies by Choi *et al*. [11]. All powders and substrate powder were created using Atomsk [27]; Manganese powder, due to its complex α-phase structure [28], was constructed as a simple BCC crystal structure and melted at 2000K and cooled to room temperature, 300K, over 1000 ps until structure reached an equilibrium. The stabilized structure was replicated and cut into a spherical powder for use in the MD study. Besides the Mn powder, the lattice parameters for other elemental powders used in the MD simulation can be found in the following Table. 1.

Table 1 Crystal Lattice Parameters for Fe, Co, Cr, Ni

Element	Crystal type	Lattice Parameter
Fe	BCC	*a = 2.871*
Co	HCP	*a = 2.507, c = 4.507*
Cr	BCC	*a = 2.91*
Ni	FCC	*a = 3.52*

The powder bed system was modeled with periodic boundary conditions in the x and y direction and a shrink wrap boundary condition in the z-direction. Initially, the system was equilibrated at 300K using an NVT ensemble for 10 ps, after which the powder bed was equilibrated at 300K using a Langevin thermostat and a canonical NVE ensemble for 10 ps. After which the substrate's temperature was controlled by a Langevin thermostat to maintain a temperature of 300K and serve as a vector of heat transfer out of the system, cooling the powder bed.

A laser scan was simulated starting at x = 80 Å and y = 143.11 Å and swept down a path in the x-direction. The laser was simulated using a heating power of 400 eV/ps over 3 different scanning velocities to determine the effect of energy density on the powder bed, and the hatch distance was set as 6 nm. All laser processing parameters can be found in Table 2.

Table 2 Laser processing parameters in this study

Test No.	Power (eV/ps)	Velocity (nm/ps)	Energy Density (J/mm^3)	Hatch Distance (nm)
1	400	0.060	46.54	6
2	400	0.045	62.06	6
3	400	0.030	93.08	6

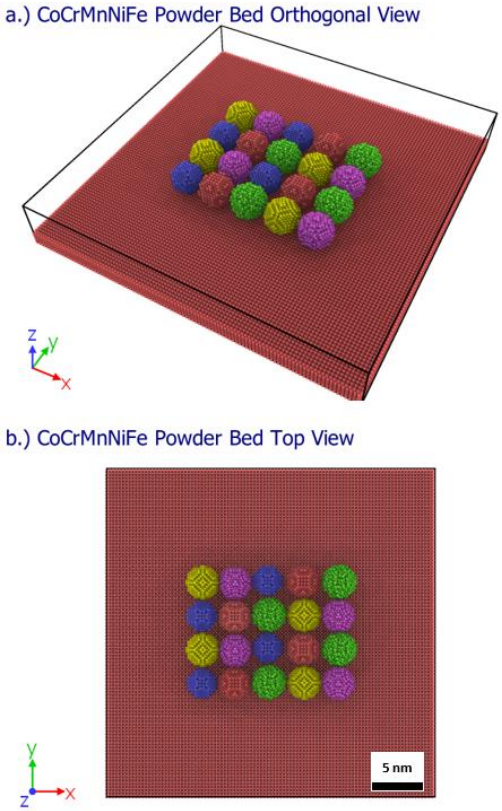

FIGURE 1: *(a) isometric view of powder bed in MD study (b) top-down view of powder bed in MD study. Powders are colored accordingly: green is Mn, yellow is Ni, blue is Cr, red is Fe, and Magenta is Co.*

3. RESULTS AND DISCUSSION

In this section, two sets of MD simulations were performed to explore the effects of diffusion of elements in HEA systems when two different laser scanning strategies were adopted.

3.1 MD study of single laser track

3.1.1 Study of laser energy density and diffusion

Figure 2 depicts the top view of the melt pool as the laser irradiates powders over time from *t=0 ps* to *t=200 ps*. Manganese powders were more unstable than their counterparts and as a result, broke apart much quicker as the heat transferred to their lattices.

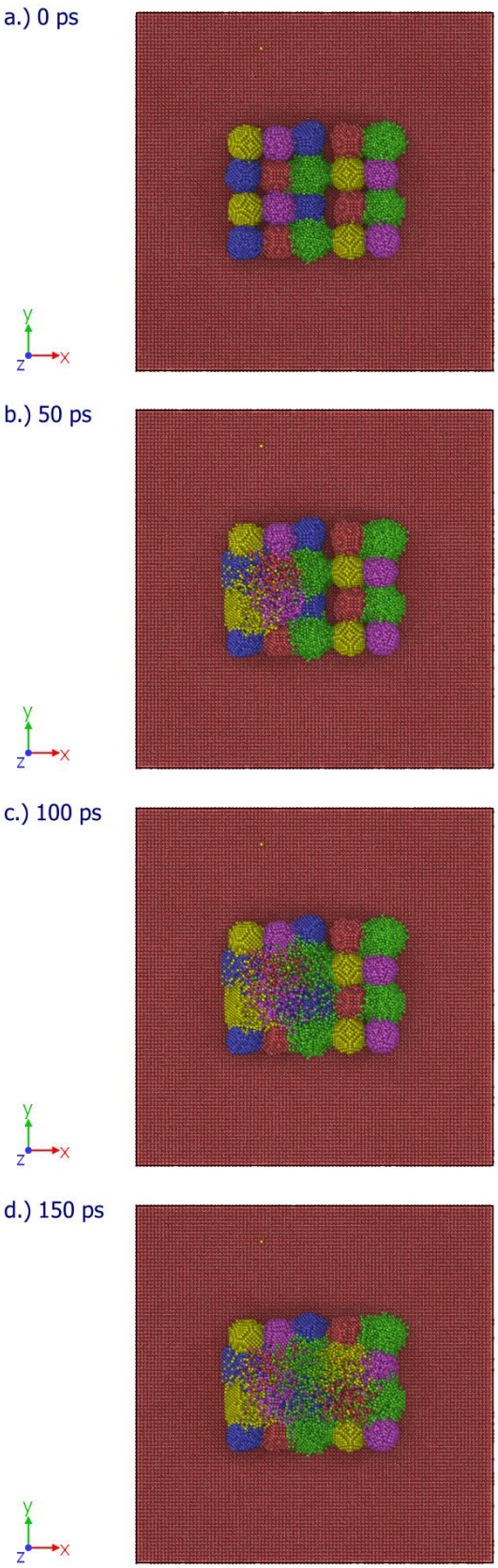

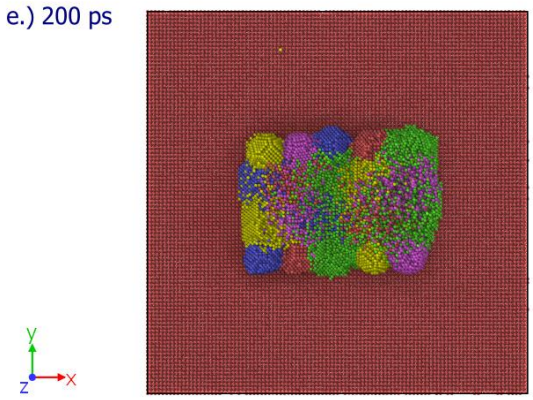

FIGURE 2: *The melting and alloying process of powder bed with a 0.06 nm/ps laser scan speed over 200 ps*

Diffusion in powder bed system is a complicated process that differs much from the ideal parameters presented in empirical approaches such as the diffusion couple or self-diffusion studies [29]. Early powder bed diffusion is driven largely by surface contact with neighboring particles [16]. A major advantage of using the MD approach is the ability to observe diffusion behavior per atom instead of through empirical methods. In this study, the Mean Squared Displacement (MSD) approach was used to study the transport of selected atoms in Figure 3, and the calculation of MSD can be written as:

$$MSD = \langle r^2(t) \rangle = \langle \frac{1}{N} \sum_{i=0}^{N} \big(r_i(t) - r_i(0)\big)^2 \rangle \qquad (2)$$

where $r_i(t) - r_i(0)$ is a vector distance traveled by a particle, N is the number of particles, and t is time. MSD can be compared among different elements with respect to their original powder cluster to gain an understanding of the occurred average displacement.

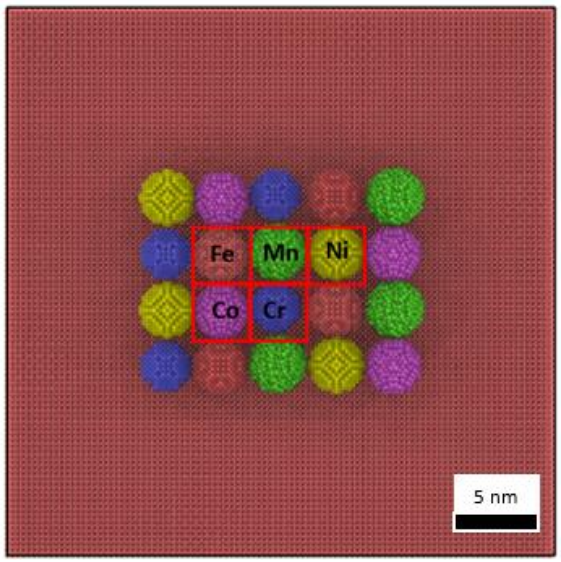

FIGURE 3: *Powders selected for study on the powder bed*

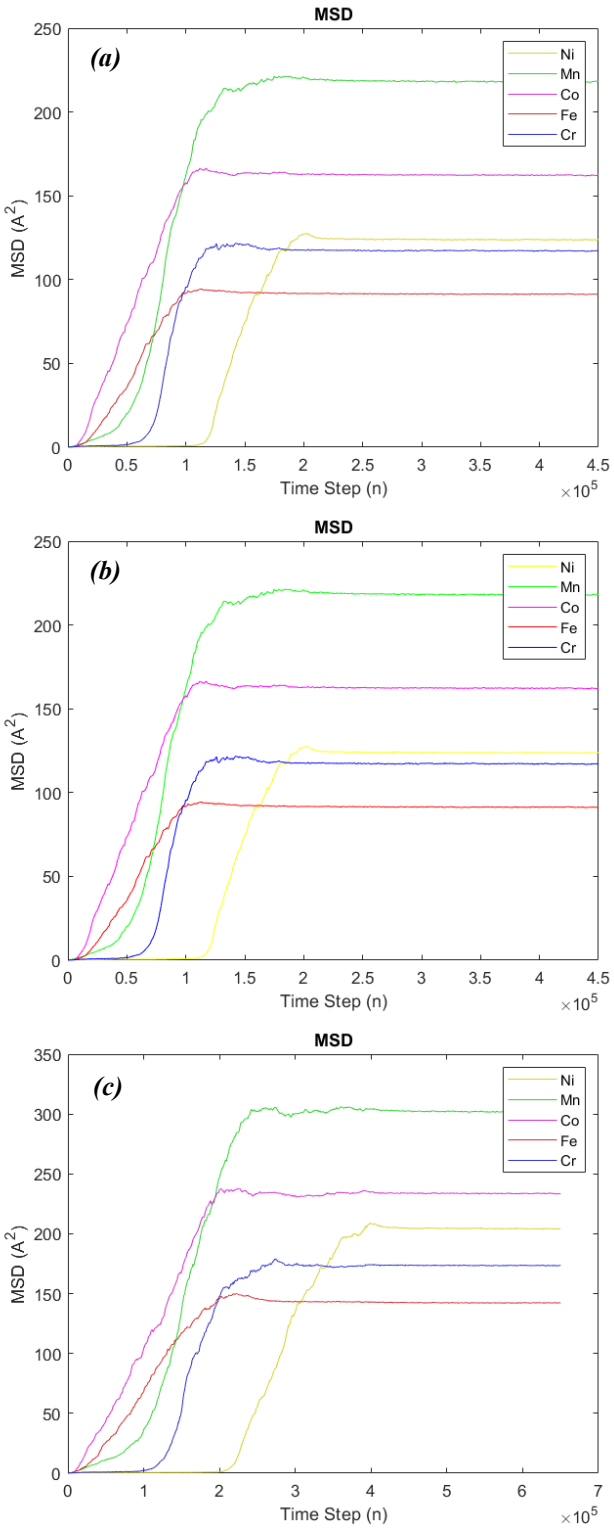

FIGURE 4: *Mean Square Displacements of selected atoms under a laser with scanning speed (a) 0.060 nm/ps, (b) 0.045 nm/ps, and (c) 0.030 nm/ps.*

MSD results were expected to exhibit non-linear mobility in the early melting process, initially, atoms dissociate from their

local lattice and move freely to fill voids in the powder bed. In the mesoscale, the different elements upon contact would experience composition driven diffusion; however, as the laser leaves a region the diffusion of the elements in the area eventually becomes minuscule as the system freezes and crystallizes, this is indicated as the MSD curve plateaus and trends towards a constant value. As shown in Figure 4, the MSD plateaus trended different constants based on the three different scanning speeds, and both Mn and Co exhibited higher MSD than the other elements of the system. In addition, slower laser scanning speed resulted in higher MSD values, which also indicated that slow scanning speed could provide more energy to local particles and promote the melting and diffusion, but there is some risk of burnout if the laser is moving too slowly.

Atomic diffusion is largely affected by the energy incident on any given atom. Moreover, the initial environment of a given atom can have a large effect on the ability of an atom to diffuse [30]. Given the initial configuration of the powder bed, the MSD of the given elements would suggest that Cr, Fe, and Ni have some difficulty in diffusing during the alloying and melting process. However, in studies by Hou *et al.* [31] it was noted that Cr has difficulty in fully melting at varying energy densities in additively manufactured FeCrCoNi alloy. This may suggest that special care should be considered when selecting these powders; for example, choosing smaller powder diameters for the given elements could help promote melting and diffusion. Based on the linear portion of each MSD curve in Figure 4b, the diffusion coefficient was calculated to roughly characterize the atomic diffusion, as shown in Table 3.

Table 3 Average Diffusion Coefficient

D ($Å^2$/ps)	Co	Cr	Fe	Mn	Ni
This Study	0.212	0.326	0.146	0.374	0.240
Ding *et al.* [20]	0.182	0.196	0.183	0.193	0.181

It is worth noting that these values were not constant and only represented the behavior in this situation. However, this is qualitatively align with results from studies with Yeh [13] and Ding [20], therefore our MD model can be verified in a reasonable range. Although it is expected that there must be a similar degree of diffusion from all constituent atoms in a system to promote homogeneity in a final product, accelerated diffusion of an element can also indicate rapid segregation, but apparently there was no observable segregation in this study.

3.1.2 Energy density and composition in single track study

Images of individual atoms were taken for each constituent element in the system, and they were then reduced to a binary image and overlayed in an in-house MATLAB program [32] to provide a qualitative analysis of diffusion throughout the powder bed by investigating the mixing of various pixels. The in-house MATLAB program can count how many different elements are existent on any single given pixel; assigning each pixel a value between 0 and 1, where 0 indicates the presence of no elements, 0.2 indicates the presence of 1 element, 0.4 the presence of 2 elements, etc. up to the maximum value of 1 which indicates the existence of 5 elements on a given pixel. According to this analysis strategy, Figure 5 shows the pixel overlay analysis for the melt powder bed under different laser scanning speeds, and this is intended to provide a topical analysis of the location where the high entropy alloy may be formed. As expected, as the laser scanning speed was lowered, there was a significant increase in pixels with 4 or 5 elements present, and the percentage of 4 and 5 element pixels in the 0.03 nm/ps laser then doubled the percentage present in the simulation using 0.06 nm/ps.

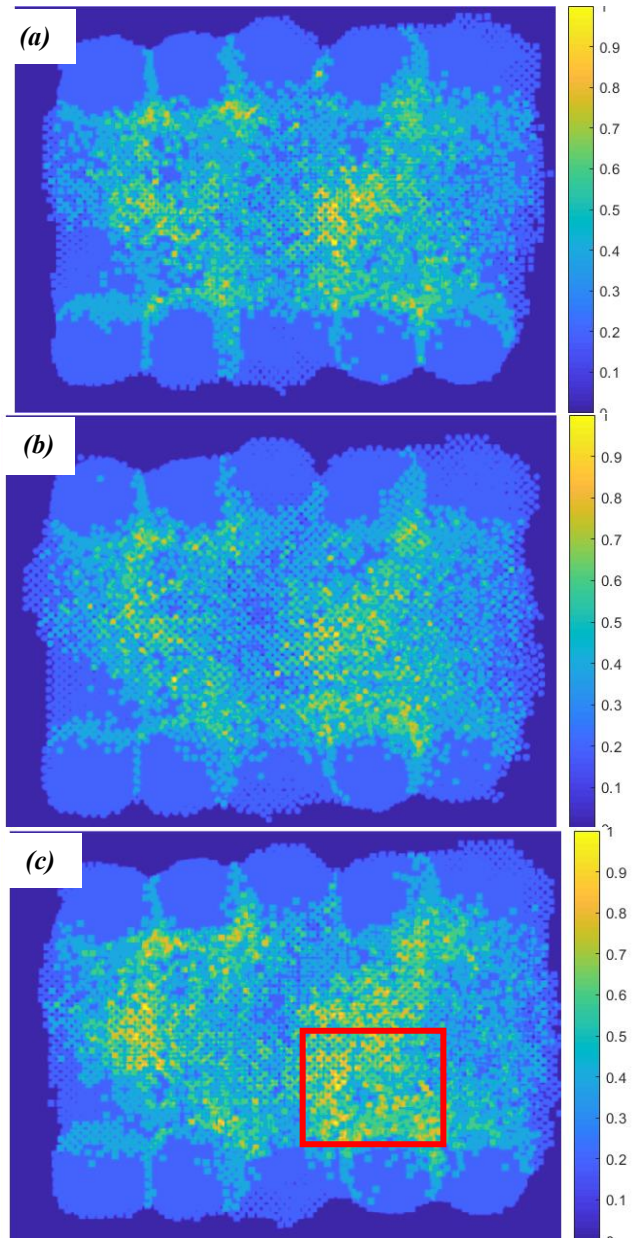

FIGURE 5: *Pixel overlays analysis of the powder bed under three different scanning speeds (a) 0.060 nm/ps; (b) 0.045 nm/ps, and (c) 0.030 nm/ps, respectively.*

As shown in Figure 5c, the indicated area shows the best pixel mixing, therefore there was a high chance that HEA would

be formed. To further analyze the material composition in the boxed area in Figure 5c, Figure 6 shows the atomic percentage of each element. Apparently, the area was expected to have a strong presence of all 4 elements, and Fe appeared in a much larger percentage as this was the original site of a Fe powder at the start of the simulation, whereas Cr was only found minimally in the location despite a Cr powder being directly adjacent to this location in the original powder configuration, as shown in Figure 3. As noted in Figures 4a and 4b, Cr and Fe exhibited the lowest MSD through the process, this may be an indication that both elemental powders may only melt for a short period before re-solidifying.

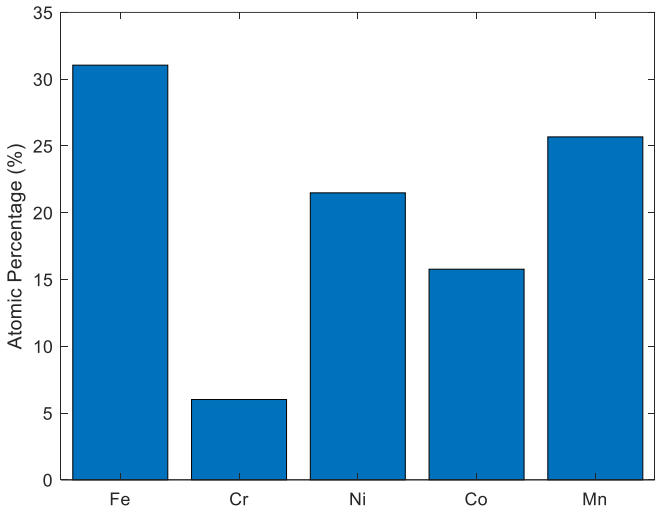

FIGURE 6: *Composition analysis of the area indicated in Figure 5c*

3.1.3 Crystal Structure of Single-Track Studies

Polyhedral Template Analysis (PTM) analysis was performed on the equilibrated, room temperature powder bed after the single laser track. In Figure 7, there was no clear change in the crystallization of the powder bed by varying the scanning speed. Furthermore, in each hatch HCP crystal was dominant over some distributed FCC crystal structure.

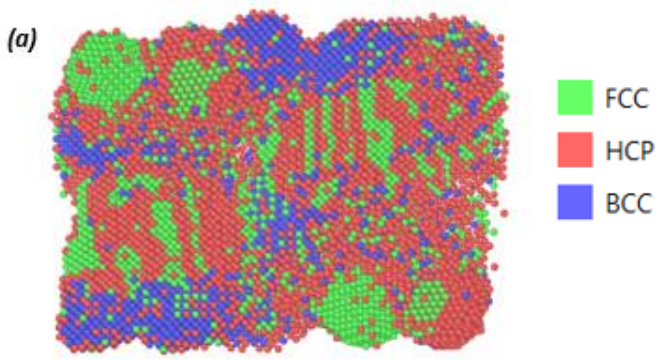

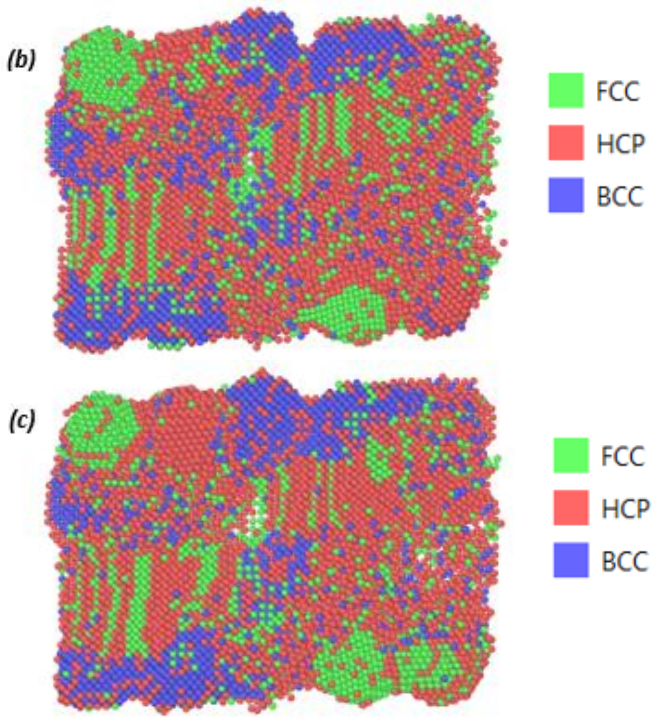

FIGURE 7: *Polyhedral Template Matching (PTM) Analysis of solidified powder bed after (a) 0.06 nm/ps (b) 0.045 nm/ps, (c) 0.03 nm/ps scanning speeds*

3.2 Multiple laser track study

3.2.1 Multiple Track Study and diffusion

Considering the best case from the single-track studies, a follow-up study was performed with 2 laser tracks operating in a meander pattern using the 0.030 nm/ps scan speed with a hatch distance of 6 nm, and the initial powder bed configuration and laser pathing can be found in Figure 8. The laser started from the upper left of the powder bed and returned from the lower right of the powder bed. There is only one present laser in the simulation at any given time, and Figure 8 displays the laser diameter and its scanning path.

Figure 9 shows the MSD result of the powder bed for two laser tracks, and it demonstrated a similar behavior as in Figure 4, in which Mn had the highest MSD overall followed by the MSD of Co and Ni. However, there was only a marginal difference of MSD between Cr and Fe. From Figure 9, we can also conclude that there was negligible diffusion after the initial laser interaction, the introduction of a second laser track also had minimal effect on the atoms which were already solidified in the first laser scan. Mn, Fe, and Ni were all introduced to the laser in the first track, but Mn was the only element experiencing notable diffusion upon the introduction of the second laser scan. However, this was mainly because Mn initially melted in the first track and then filled in voids in its adjacent powders, therefore much more Mn atoms were excited by the second laser track.

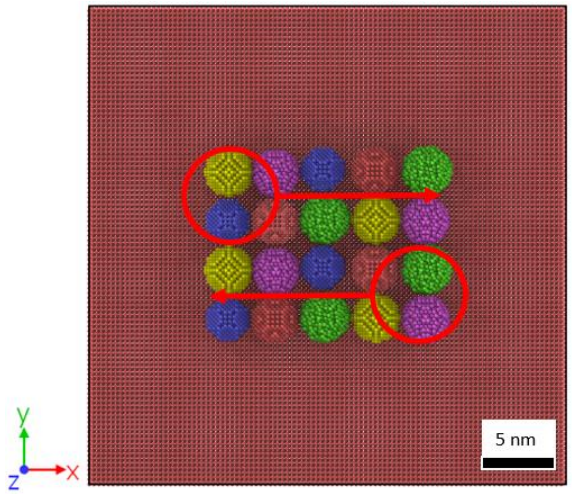

FIGURE 8: *Initial powder bed configuration and laser pathing for two laser tracks*

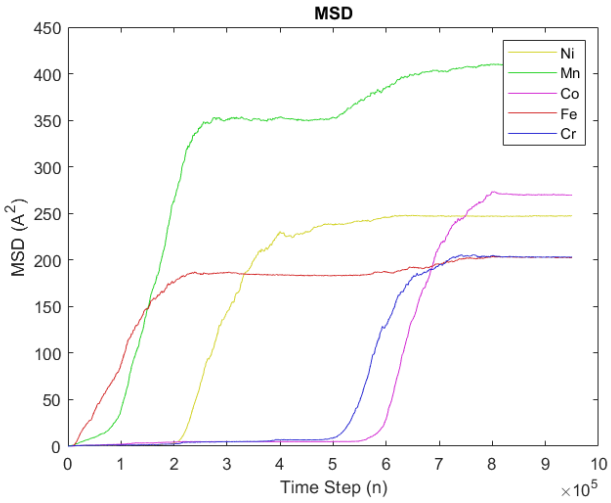

FIGURE 9: *Mean Square Displacements of atoms selected under two subsequent laser tracks traveling at 0.03 nm/ps*

3.2.2 Multiple Track Study Composition

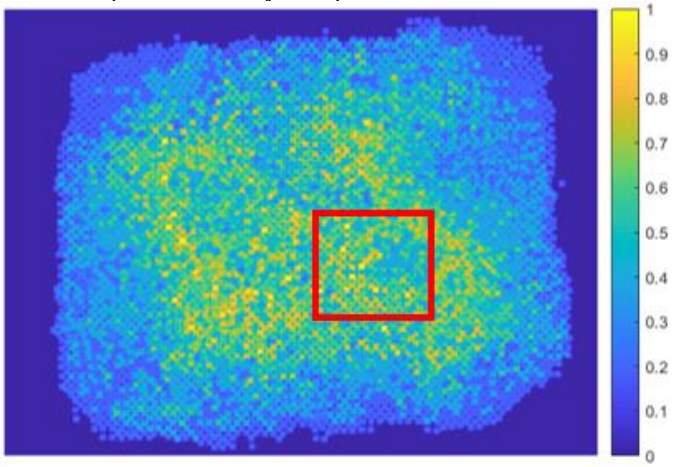

FIGURE 10: *Pixel overlay analysis of two laser track simulation using a meander hatch strategy.*

The pixel overlay analysis in Figure 10 shows that there was no noticeable increase of areas where 4 or 5 elements appeared on the powder bed after two laser tracks. Figure 11 analyzes the compositions of various elements in the boxed area in Figure 10, and the location of the boxed area was the same as in Figure 5c. Figure 11 shows that Fe, Ni, and Mn all appeared in almost identical atomic ratio, both Cr and Co appeared in a lower concentration, but Cr had slightly higher concentration than Co. Considering the two track scanning strategy, many atoms, especially on the boundary of the powder bed, had more freedom to mobilize because of more laser energy input. The change in laser strategy enabled different powders to interact, directly changing the composition of any given area on the powder bed.

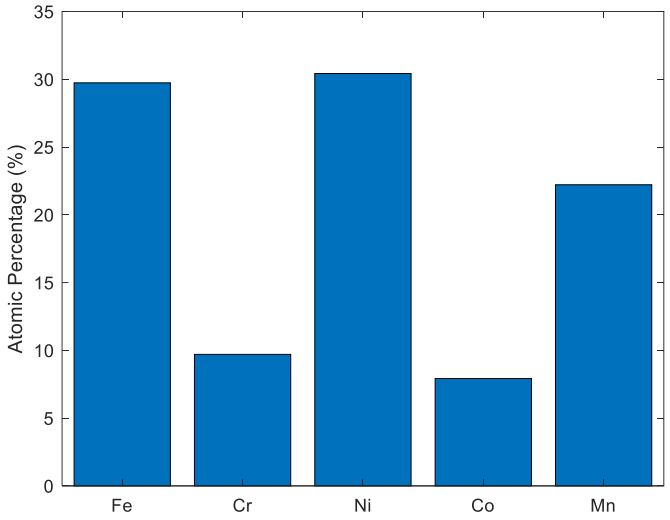

FIGURE 11: *Composition analysis of the boxed area in Figure 10*

3.2.3 Crystallization of Powder Bed

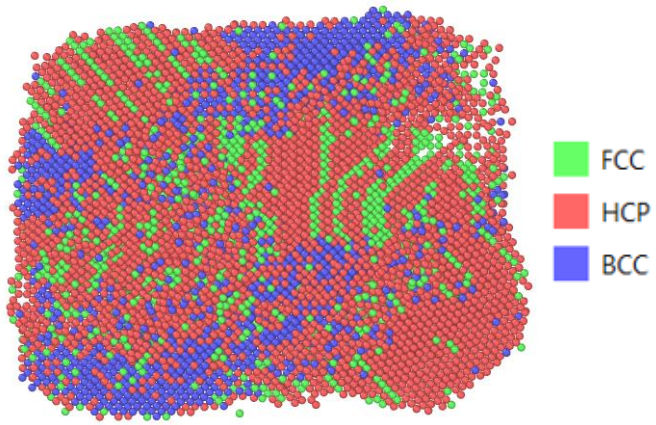

FIGURE 11: *PTM Analysis of solidified powder bed after 2 track meander scanning*

Through the PTM analysis for Figure 10, Figure 11 demonstrates that the pure FCC crystal structure, which was desired to be observed as an indication of Cantor HEA

formation, showed up in the center of the powder bed. However, the HCP crystal structure was dominant over the FCC and BCC structures. A potential resolution to form more FCC structure is to apply higher laser energy, slower laser scanning speed, and a more controlled cooling rate, therefore the mobility of atoms in the melt pool can be increased by allowing for more thorough diffusion, assuming the effects of segregation during cooling stage is negligible.

4. CONCLUSION

In this study, MD study was performed to simulate the *in-situ* alloying using elemental powders, in order to obtain a good understanding of the effect of diffusion on the formation of Cantor HEA. The framework developed in this work can be used to explore the effect of diffusion on the thermomechanical properties of HEAs, and to design other HEA systems by considering the most appropriate manufacturing process parameters. The major findings of this study are summarized as follows:

1) All the elements experience different MSDs during the laser scanning process. Not only was diffusion rate different among various elements, but the active time of diffusing also differed. However, the diffusion process may be largely influenced by the configuration of the powder bed;
2) All powders experienced the same tendency in terms of MSD despite different laser scanning speeds introduced to the powder bed system;
3) Cr and Fe both exhibited minimal diffusion compared to other constituent elements (Mn, Ni, and Co), resulting in areas where 3 or 4 elements were present in near equiatomic compositions;
4) The study of single laser track shows more FCC structures than the double laser track, therefore it is expected that more Cantor HEA was formed during the process, therefore it needs more investigation to explore the relationship between the formation of HEA and the input laser energy, as well as other related parameters.

ACKNOWLEDGEMENTS

This work is supported by US Department of Defense Manufacturing Engineering Education Program (MEEP) under the award # N00014-19-1-2728, the Bose Family Donation to the Department of Manufacturing and Industrial Engineering at UTRGV, and the start-up fund at Mississippi State University. This work used the Extreme Science and Engineering Discovery Environment (XSEDE) Stampede2 at TACC through allocation TG-CTS200013 and Bridges2 at PSC through allocation TG-MCH200010, supported by National Science Foundation grant number ACI-1548562.

NOMENCLATURE

AM	Additive Manufacturing
Co	Cobalt
Cr	Chromium
EAM	Embedded Atom Method
Fe	Iron
HEA	High Entropy Alloy
MD	Molecular Dynamics
MEAM	Modified Embedded Atom Method
Mn	Manganese
Ni	Nickel
p*	Laser Power
SLM	Selective Laser Melting
SLA	Selective Laser Alloying
LAA	Laser Additive Alloying
v_s	laser scanning speed (nm/s)

REFERENCES

.[1] Y. Zhang *et al.*, “Microstructures and properties of high-entropy alloys,” *Progress in Materials Science*, vol. 61. Elsevier Ltd, pp. 1–93, Apr. 01, 2014, doi: 10.1016/j.pmatsci.2013.10.001.

[2] J. W. Yeh *et al.*, “Nanostructured high-entropy alloys with multiple principal elements: Novel alloy design concepts and outcomes,” *Adv. Eng. Mater.*, vol. 6, no. 5, pp. 299–303, May 2004, doi: 10.1002/adem.200300567.

[3] B. Cantor, I. T. H. Chang, P. Knight, and A. J. B. Vincent, “Microstructural development in equiatomic multicomponent alloys,” *Mater. Sci. Eng. A*, vol. 375–377, no. 1-2 SPEC. ISS., pp. 213–218, Jul. 2004, doi: 10.1016/j.msea.2003.10.257.

[4] M. H. Chuang, M. H. Tsai, W. R. Wang, S. J. Lin, and J. W. Yeh, “Microstructure and wear behavior of AlxCo 1.5CrFeNi1.5Tiy high-entropy alloys,” *Acta Mater.*, vol. 59, no. 16, pp. 6308–6317, Sep. 2011, doi: 10.1016/j.actamat.2011.06.041.

[5] O. N. Senkov, G. B. Wilks, J. M. Scott, and D. B. Miracle, “Mechanical properties of Nb25Mo25Ta 25W25 and V20Nb20Mo 20Ta20W20 refractory high entropy alloys,” *Intermetallics*, vol. 19, no. 5, pp. 698–706, May 2011, doi: 10.1016/j.intermet.2011.01.004.

[6] C. Sha, Z. Zhou, Z. Xie, and P. Munroe, “Extremely hard, α-Mn type high entropy alloy coatings,” *Scr. Mater.*, vol. 178, pp. 477–482, Mar. 2020, doi: 10.1016/j.scriptamat.2019.12.029.

[7] Y. L. Chou, Y. C. Wang, J. W. Yeh, and H. C. Shih, “Pitting corrosion of the high-entropy alloy Co1.5CrFeNi1.5Ti0.5Mo0.1 in chloride-containing sulphate solutions,” *Corros. Sci.*, vol. 52, no. 10, pp. 3481–3491, Oct. 2010, doi: 10.1016/j.corsci.2010.06.025.

[8] M. H. Tsai, “Physical properties of high entropy alloys,” *Entropy*, vol. 15, no. 12. MDPI AG, pp. 5338–5345, Dec. 03, 2013, doi: 10.3390/e15125338.

[9] E. J. Pickering, R. Muñoz-Moreno, H. J. Stone, and N. G. Jones, “Precipitation in the equiatomic high-entropy alloy CrMnFeCoNi,” *Scr. Mater.*, vol. 113, pp. 106–109, Mar. 2016, doi: 10.1016/j.scriptamat.2015.10.025.

[10] D. B. Miracle and O. N. Senkov, “A critical review of high entropy alloys and related concepts,” *Acta Materialia*, vol. 122. Elsevier Ltd, pp. 448–511, Jan. 01, 2017, doi: 10.1016/j.actamat.2016.08.081.

[11] W. M. Choi, Y. H. Jo, S. S. Sohn, S. Lee, and B. J. Lee, "Understanding the physical metallurgy of the CoCrFeMnNi high-entropy alloy: An atomistic simulation study," *npj Comput. Mater.*, vol. 4, no. 1, p. 1, Dec. 2018, doi: 10.1038/s41524-017-0060-9.

[12] M. H. Mosallanejad, B. Niroumand, A. Aversa, and A. Saboori, "In-situ alloying in laser-based additive manufacturing processes: A critical review," *J. Alloys Compd.*, vol. 872, p. 159567, Aug. 2021, doi: 10.1016/j.jallcom.2021.159567.

[13] K. Y. Tsai, M. H. Tsai, and J. W. Yeh, "Sluggish diffusion in Co-Cr-Fe-Mn-Ni high-entropy alloys," *Acta Mater.*, vol. 61, no. 13, pp. 4887–4897, Aug. 2013, doi: 10.1016/j.actamat.2013.04.058.

[14] J. Dąbrowa *et al.*, "Demystifying the sluggish diffusion effect in high entropy alloys," *J. Alloys Compd.*, vol. 783, pp. 193–207, Apr. 2019, doi: 10.1016/j.jallcom.2018.12.300.

[15] C. G. Schön, M. A. Tunes, R. Arróyave, and J. Ågren, "On the complexity of solid-state diffusion in highly concentrated alloys and the sluggish diffusion core-effect," *Calphad Comput. Coupling Phase Diagrams Thermochem.*, vol. 68, p. 101713, Mar. 2020, doi: 10.1016/j.calphad.2019.101713.

[16] F. Wakai, "Modeling and simulation of elementary processes in ideal sintering," *J. Am. Ceram. Soc.*, vol. 89, no. 5, pp. 1471–1484, May 2006, doi: 10.1111/j.1551-2916.2006.01001.x.

[17] J. Nandy, N. Yedla, P. Gupta, H. Sarangi, and S. Sahoo, "Sintering of AlSi10Mg particles in direct metal laser sintering process: A molecular dynamics simulation study," *Mater. Chem. Phys.*, vol. 236, p. 121803, Oct. 2019, doi: 10.1016/j.matchemphys.2019.121803.

[18] L. Yang, Y. Gan, Y. Zhang, and J. K. Chen, "Molecular dynamics simulation of neck growth in laser sintering of different-sized gold nanoparticles under different heating rates," *Appl. Phys. A Mater. Sci. Process.*, vol. 106, no. 3, pp. 725–735, Mar. 2012, doi: 10.1007/s00339-011-6680-x.

[19] H. Chen, Q. Fang, K. Zhou, Y. Liu, and J. Li, "Unraveling atomic-scale crystallization and microstructural evolution of a selective laser melted FeCrNi medium-entropy alloy," *CrystEngComm*, vol. 22, no. 24, pp. 4136–4146, Jun. 2020, doi: 10.1039/d0ce00358a.

[20] J. Ding, M. Asta, and R. O. Ritchie, "Melts of CrCoNi-based high-entropy alloys: Atomic diffusion and electronic/atomic structure from ab initio simulation," *Appl. Phys. Lett.*, vol. 113, no. 11, p. 111902, Sep. 2018, doi: 10.1063/1.5045216.

[21] S. Guo, M. Wang, Z. Zhao, Y. Y. Zhang, X. Lin, and W. D. Huang, "Molecular dynamics simulation on the micro-structural evolution in heat-affected zone during the preparation of bulk metallic glasses with selective laser melting," *J. Alloys Compd.*, vol. 697, pp. 443–449, Mar. 2017, doi: 10.1016/j.jallcom.2016.11.393.

[22] Y. Zhang *et al.*, "Atomic-level crystallization in selective laser melting fabricated Zr-based metallic glasses," *Phys. Chem. Chem. Phys.*, vol. 21, no. 23, pp. 12406–12413, 2019, doi: 10.1039/c9cp02181g.

[23] S. Kurian and R. Mirzaeifar, "Selective laser melting of aluminum nano-powder particles, a molecular dynamics study," *Addit. Manuf.*, vol. 35, p. 101272, Oct. 2020, doi: 10.1016/j.addma.2020.101272.

[24] S. Plimpton, "Fast Parallel Algorithms for Short-Range Molecular Dynamics," 1995. Accessed: Apr. 27, 2021. [Online]. Available: http://www.cs.sandia.gov/~sjplimp/main.html.

[25] "LAMMPS Molecular Dynamics Simulator." https://lammps.sandia.gov/ (accessed Apr. 28, 2021).

[26] A. Stukowski, "Visualization and analysis of atomistic simulation data with OVITO-the Open Visualization Tool," *Model. Simul. Mater. Sci. Eng.*, vol. 18, no. 1, Jan. 2010, doi: 10.1088/0965-0393/18/1/015012.

[27] P. Hirel, "Atomsk: A tool for manipulating and converting atomic data files," *Comput. Phys. Commun.*, vol. 197, pp. 212–219, Dec. 2015, doi: 10.1016/j.cpc.2015.07.012.

[28] D. Hobbs, J. Hafner, and D. Spišák, "Understanding the complex metallic element Mn. I. Crystalline and noncollinear magnetic structure of α-Mn," *Phys. Rev. B*, vol. 68, no. 1, p. 014407, Jul. 2003, doi: 10.1103/PhysRevB.68.014407.

[29] P. Song and D. Wen, "Molecular dynamics simulation of the sintering of metallic nanoparticles," *J. Nanoparticle Res.*, vol. 12, no. 3, pp. 823–829, Mar. 2010, doi: 10.1007/s11051-009-9718-7.

[30] C. Zener, "Theory of Do for atomic diffusion in metals," *J. Appl. Phys.*, vol. 22, no. 4, pp. 372–375, 1951, doi: 10.1063/1.1699967.

[31] Y. Hou, H. Su, H. Zhang, X. Wang, and C. Wang, "Fabricating homogeneous fecocrni high-entropy alloys via slm in situ alloying," *Metals (Basel).*, vol. 11, no. 6, p. 942, Jun. 2021, doi: 10.3390/met11060942.

[32] "MATLAB version 9.6.0.1174912 (R2019a) Update 5." Natick, Massachusetts, 2019.